frontiers | Frontiers in Energy Research

TYPE Methods
PUBLISHED 27 March 2024
DOI 10.3389/fenrg.2024.1375831

OPEN ACCESS

EDITED BY
Fei Wang,
Qingdao University of Science and Technology, China

REVIEWED BY
Roshan Raman,
The Northcap University, India
Xiukun Wang,
China University of Petroleum, Beijing, China

*CORRESPONDENCE
Shuang Zhao,
zhao163shuang@163.com

RECEIVED 25 January 2024
ACCEPTED 04 March 2024
PUBLISHED 27 March 2024

CITATION
Lang L, Zhao S and Liu L (2024), Experimental study of ultra-low IFT foam flooding for low permeability reservoirs.
Front. Energy Res. 12:1375831.
doi: 10.3389/fenrg.2024.1375831

Experimental study of ultra-low IFT foam flooding for low permeability reservoirs

Liyuan Lang, Shuang Zhao* and Lu Liu

SINOPEC Southwest Oil and Gas Company, Exploration and Development Research Institute, Chengdu, Sichuan, China

Foam flooding is an effective oil displacement technique to improve fluid sweep efficiency and increase oil recovery. The objective of this paper is to investigate the applicability of ultra-low IFT foam flooding for low permeability oil recovery under the conditions of WX reservoir block in Tuha oilfield (84°C, 86,072 mg/L). A modified amphoteric hydroxy sulfobetaine surfactant (Cn-HSB) was formulated as a foaming agent based on the principle of compatibility with crude oil that could achieve the ultra-low interfacial tension (IFT) and strong foamability simultaneously. This is shown to reduce the oil/water dynamic IFT (DIFT) to an ultra-low value of the order of 10^{-5} mN/m (0.10*wt*%), as well as produce a foam volume and half-life of 448 mL and 2567 s, respectively. In addition, results of IFT and foam quality tests indicate that the modified Cn-HSB has good thermal stability and excellent salinity-resistance. Moreover, the ultra-low IFT foam flooding has an ideal injectivity and oil displacement efficiency in low permeability porous media that can mobilize the trapped oil in k = 1.50 × 10^{-3}μm^2 with a threshold pressure gradient of 0.115 MPa/m. This improves oil displacement efficiency about 15%OOIP. Fundamental knowledge gained from this research gives insight into the application of ultra-low IFT foam flooding in low-permeability reservoirs under a combination of specific reservoir conditions.

KEYWORDS

foam flooding, surfactant, low permeability, interfacial tension, enhance oil recovery

1 Introduction

In 2021, the oil production of China was 1.99 × 10^8t, while the net oil import volume was 5.13 × 10^8t. It demonstrates that a total of over 70% of China's oil usage is dependent on imported oil. It is urgent to speed up the oil exploration and development to meet growing demands. According to the fourth Evaluation of Petroleum Reserves and Resources in 2016, low permeability oil reserves accounted for 78% as of 2011, that percentage increased to 94% in 2017 with the discovery of additional oil deposits. As of the end of 2020, the cumulative proven oil reserves in China is estimated to be 422 × 10^8t, and above 60% of that oil is in low permeability reservoirs that are the widely distributed across twenty-one oil fields in China (Li et al., 2020). It is clear that the low permeability resources have played a significant role in exploration and development of Chinese oilfield in recent years, making the efficient exploitation of low permeability resources a vital strategic goal for sustainable petroleum development.

The low-permeability reservoirs generally demonstrate the following poor physical properties:serious heterogeneity, high capillary pressure, the large resistance of Jamin effect, etc., resulting in insufficient water-injection, which greatly restricts the efficiency of conventional water flooding technology to 15%~25% (Yu et al., 2015). Meanwhile, gas

TABLE 1 Theoretic calculation of the minimum IFT for mobilizing the capillary trapped residual oil.

r (μm)	k (×10^{-3}μm^2)	L (cm)	IFT (mN/m)			
			θ_O = 17°	θ_O = 41°	θ_O = 78°	θ_O = 85°
0.05	0.005	0.002	2.09×10^{-5}	2.65×10^{-5}	9.62×10^{-5}	2.29×10^{-4}
0.10	0.02	0.002	4.18×10^{-5}	5.30×10^{-5}	1.92×10^{-4}	4.59×10^{-4}
0.25	0.125	0.002	1.05×10^{-4}	1.33×10^{-4}	4.81×10^{-4}	1.15×10^{-3}
0.50	0.5	0.002	2.09×10^{-4}	2.65×10^{-4}	9.62×10^{-4}	2.30×10^{-3}
1.0	2	0.002	4.18×10^{-4}	5.30×10^{-4}	1.92×10^{-3}	4.59×10^{-3}
2.0	8	0.002	8.37×10^{-4}	1.06×10^{-3}	3.85×10^{-3}	9.18×10^{-3}
3.0	18	0.002	1.26×10^{-3}	1.59×10^{-3}	5.77×10^{-3}	1.38×10^{-2}
5.0	50	0.002	2.09×10^{-3}	2.65×10^{-3}	9.62×10^{-3}	2.29×10^{-2}
7.0	98	0.002	2.93×10^{-3}	3.71×10^{-3}	1.35×10^{-2}	3.21×10^{-2}
9.0	162	0.002	3.77×10^{-3}	4.77×10^{-3}	1.73×10^{-2}	4.13×10^{-2}

TABLE 2 The pros and cons of main recovery methods in low permeability reservoirs.

Method	Benefits	Key issues	EOR (% OOIP)
Water Flooding	economical	difficulty in injection (because of low permeability, water-sensitive, etc.)	5~20
Gas Injection	ideal injectivity	①lack of gas source	3~10
		②gas breakthrough (poor sweep efficiency)	
Chemical EOR (e.g.,.ASP or SP)	been successfully used in medium and high permeability reservoir (k ≥ 50 × 10^{-3}μm^2)	①difficulty in injection (due to the flooding system contain polymer)	about 20
		②chemical degradation	
		③higher chemical adsorption	
Foam Flooding (general)	foaming agent	cannot improve the displacement efficiency in low permeability reservoir (the order of IFT from 10^{-1} mN/m to 10^{-3} mN/m)	about 15
	①high apparent viscosity (improve the sweep efficiency)		
	②favorable mobility control		
	③injectability		

flooding is a widely used EOR technique because of its ideal injection properties, but gas breakthrough results in unfavorable mobility control in serious heterogeneity reservoirs, contributing to the poor sweep efficiency. So large amount of oil remains trapped underground after primary and secondary recovery process.

In addition, the application of chemical EOR methods (e.g.,.ASP or SP) was proven to be successful in medium and high permeability reservoir (k ≥ 50 × 10^{-3}μm^2)in the early 1990s in China, which based on the mechanisms of reducing IFT and improving sweep efficiency. However, for the low permeability reservoirs, the addition of polymer face three main issues: difficulty in injection, chemical degradation, especially in harsh conditions, and higher chemical adsorption due to the larger specific surface area of low permeability reservoirs. Moreover, although the IFT can fall to the order of 10^{-3} mN/m (Wang and Cheng, 2001), the capillary trapped residual oil in low permeability reservoirs cannot be extracted that the displacement efficiency cannot be improved. Due to the need to mobilize the capillary trapped residual oil, it is necessary to integrate $\Delta P \geq P_c$ into the theoretical calculation of the minimum IFT as demonstrated by the following Eqs 1–4, the results of this integration are listed in Table 1.

$$Pc = \frac{2\sigma}{r}\cos\theta_o \tag{1}$$

$$\Delta P = \frac{dP}{dx} \cdot L \tag{2}$$

$$\sigma \leq \frac{1}{2\cos\theta_o} r \cdot \left(\frac{dP}{dx} \cdot L\right) \tag{3}$$

$$k = r^2 \frac{\phi}{8\tau^2} \tag{4}$$

where P_c is capillary pressure, MPa; ΔP is driving force, MPa; σ is the oil/water IFT, mN/m; θ_o is the contact angle of oil phase, °; r is the radius of pore throat, μm; ϕ is porosity, %; k is the permeability, ×10^{-3}μm^2; τ is the tortuosity; L is the length of an oil droplet, cm.

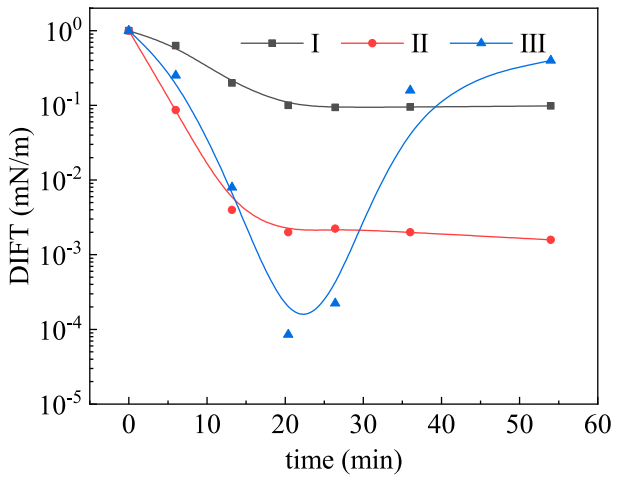

FIGURE 1
The variation characteristics of oil/water DIFT.

As we can see from Table 1, the more the reservoir rock trends to water wettability and the lower the permeability, the lower the theoretical calculation of the IFT minima necessary for mobilizing the capillary trapped residual oil it is necessary. When $k \leq 50 \times 10^{-3}$ m^2, mobilizing this oil is achieved by reducing the oil/water IFT to an ultra-low level (10^{-3} mN/m to 10^{-5} mN/m). It must be said that it is very difficult to get a surfactant with ultra-low equilibrium IFT (EIFT) of the order of 10^{-3} mN/m to 10^{-5} mN/m. However, it is easier to achieve such ultra-low value with DIFT.

The main benefits and detriments of different oil recovery methods are listed in Table 2. These issues have made the exploration of low permeability oil reservoirs technically challenging. Therefore, ultra-low IFT foaming agent of the injected gas (N_2, CO_2, air, ect.) is regarded as a feasible technique for low-permeability reservoirs development. Nevertheless, it is crucial to formulate an effective foaming agent that can both improve oil displacement efficiency and the sweep efficiency by achieving the ultra-low IFT and strong foamability simultaneously. Reaching this goal has been challenging.

The possibility of dynamic IFT minima was first put forward by Wilson and Ries (Rubin and Radke, 1980) in 1923. Later, Ward and Tordai gave a quantitative description of the diffusion effect on dynamic IFT behavior in 1944. After that, some scholars (Rubin and Radke, 1980; Trujillo, 1983; Cambridge et al., 1989; Sharma et al., 1989), started to research on the dynamic IFT behavior in chemical flooding experiments. In some of the previous studies the variation characteristics of oil/water DIFT can be classified into three features, as shown in Figure 1. Taylor and Schramm, (1990) reported the effect of dynamic IFT minimum is responsible for improving the displacement efficiency. More recently, some Chinese researchers studied the improvement of oil displacement efficiency based on the same order of magnitude of equilibrium and dynamic IFT in ASP flooding by core flooding tests under the reservoir conditions of Daqing oilfield ($k \geq 50 \times 10^{-3}$ m^2). The results demonstrated that DIFT minimum was the key to mobilizing trapped oil in porous media which showed an improvement of 20%OOIP after water flooding. A possible theoretical explanation is that the ultra-low oil/water DIFT may develop in a short time, after which the residual oil was displaced to form a continuous "oil bank," creating a snowball effect of growth which gathers more residual oil as it advances.

In this study, we selected the WX reservoir block (temperature 84°C, brine salinity 86,072 mg/L, average permeability $k = 27.6 \times 10^{-3}$μm^2) in Tuha oilfield as an example. Firstly, based on the principle of compatibility with crude oil, the novel temperature-resistant, salinity-resistant, ultra-low IFT foaming agent was formulated with specific focus on the design of molecular structure. Meanwhile, experiments under the reservoir conditions were carried out to evaluate its properties, including IFT and foam property. Following that, a series of core flooding experiments were carried out to investigate the injection capacity and displacement efficiency of ultra-low IFT foam flooding for low permeability oil recovery.

2 Experimental section

2.1 Materials

2.1.1 Crude oil

The crude oil sample was obtained from an oil block of the WX well area in the Tuha oilfield (Xinjiang, China). The viscosity of the oil sample is 4.9 mPa s and the oil density is 0.626 g/cm^3 at 84°C. The crude oil was filtered through a 5 μm filter to remove solids and contaminants before all tests.

2.1.2 Brines

Synthetic formation brine was prepared in this study. The composition of the synthetic brine is listed in Table 3.

All tests were performed at 84°C to simulate the temperature of the applicable reservoir and distilled water was used for the preparation of all aqueous solutions.

2.1.3 Chemical agent

The modified betaine-type amphoteric surfactant (Cn-HSB) was formulated on the basis of the designing of molecular structure according to the principle of compatibility with crude oil, with the cooperation of Huayangxinghua Chemical Industry Co., Ltd. (Chengdu, China).

2.1.4 Core sample

For the core flooding tests, the natural sandstone core samples are taken from WX reservoir block, with its characteristic permeability is from 0.1 × 10^{-3}μm^{2}to 50 × 10^{-3}μm^2. The artificial core samples are purchased from Northeast Petroleum University.

TABLE 3 Composition of the synthetic formation brine.

Ions	Na^+	Ca^{2+}	Mg^{2+}	Cl^-	SO_4^{2-}	HCO_3^-	TDS
concentration (mg/L)	23,374	7548	1300	51,165	2568	117	86,072

Where TDS, is Total Dissolved Solids which means the salinity of the formation water.

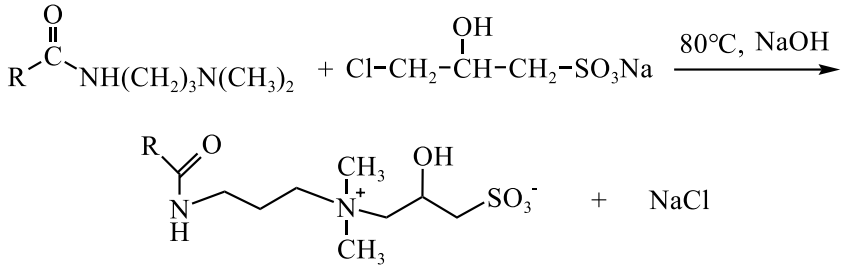

SCHEME 1
Route of synthesizing the modified Cn-HSB (*n* = 12~18) by quaternarization.

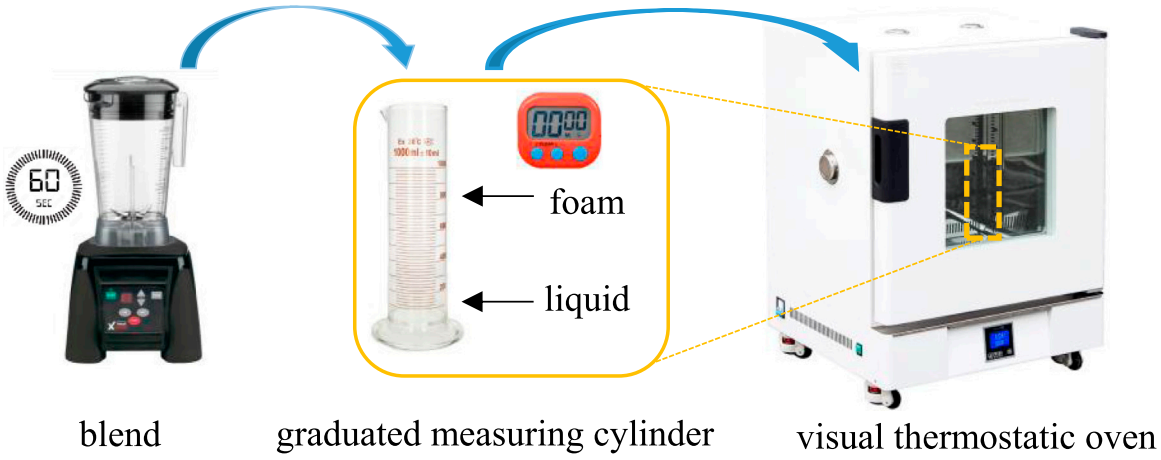

FIGURE 2
The procedure of foamability test.

2.2 Experiment procedure

2.2.1 Synthesis of Cn-HSB

The synthesis of the modified Cn-HSB is outlined below in Scheme 1. The 3-chloro-2-hydroxypropanesulfonic acid sodium and isopropyl alcohol were successively injected into a three-necked flask, using sodium hydroxide (NaOH) as catalyst, and subsequently heated in a water bath at 80°C for 2 h, maintain pH within 7 ~8. When it began to reflux, alkyl amido propyl dimethylamine was slowly added into the system. After 8 h of reaction, the results of the reaction were determined by the percentage of conversion of alkyl amido propyl dimethylamine to above 90%, the product was obtained when the solvent (isopropyl alcohol) was removed using rotary evaporation. Further purification with anhydrous ethanol through washing and drying were repeated three times.

2.2.2 Structural characterization of crude oil and foaming agent

The distribution of hydrocarbon composition in crude oil was tested by Gas Chromatography-Mass Spectrometer (GC-MS). Accordingly, GC-MS spectra was recorded with TSQ Quantum.

The molecule was structurally characterized by Fourier Transform Infrared Spectroscopy (FT-IR) and Nuclear Magnetic Resonance Spectroscopy (^{1}H NMR). The FT-IR spectra were analyzed using a Thermo Scientific™ Nicolet™ iS™10 FTIR Spectrometer. 1H NMR spectra were recorded with a BRUKER UltrShieldAVANCE 300 MHz spectrometer, using D2O as solvent. The thermogravimetry was measured by METTLER TOLEDOTGA/DSC2/1100LF and conducted under nitrogen (N2) atmosphere at a heating rate of 10.00K/min.

2.2.3 Foamability and foam-stability tests

The Waring Blender method is commonly used to evaluate the foamability. The experimental procedure is as follows (Figure 2): firstly, 100 mL of different concentrations of foaming agent solution were prepared and the oven was preheated to the 84°C. Then the solution was poured into the blender, stirring for 60 s at a rotating speed of 8,000 r/min. The bulk foam was put into a 1,000 mL graduated measuring cylinder that should be sealed with plastic wrap rapidly and then placed into a visual thermostatic oven. Finally, the decay of foam was observed over time, recording the foam volume and half-life duration, the foam composite index (*FCI*) was used as well to determine the stability of the generated foam, it is defined as Eq. 5:

$$FCI = \frac{3}{4} t_{\frac{1}{2}} \cdot V_{max} \quad (5)$$

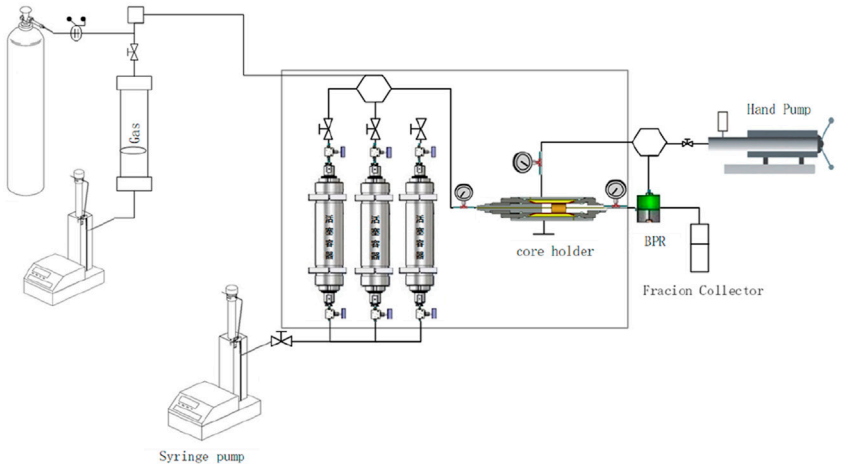

FIGURE 3
Schematic core flooding apparatus.

where V_{max} is the maximum foam volume, mL; $t_{1/2}$ is half-life of foam, s;

Meanwhile, the high-temperature and high-pressure foam evaluation device (Halan oil scientific instrument CO., LTD) was used.

2.2.4 Measurement of interfacial tension

The IFT between the surfactants solutions and crude oil were measured by TX500C interfacial tensiometer (Shanghai Zhongchen Instrument Company, China) using the spinning drop method at 84°C. The rotating speed was fixed at 6,000 r/min.

2.2.5 Oil displacement performance

The experimental setup is presented schematically in Figure 3.

A series of core flooding experiments were carried out at 84°C by an oil displacement physical simulation device by following the steps:

(1) The properties of low permeability cores were measured.
(2) The cores were saturated with synthetic formation brine under vacuum, and the pore volume, porosity, and permeability of the core samples were determined.
(3) The cores were saturated with crude oil at a constant flow rate of 0.01 mL/min until no water was observed and the oil saturation was calculated.
(4) The water flooding was conducted until negligible amounts of oil were produced.
(5) 0.3 pore volume (PV) of displacement slug was used to flood the residual oil. Then the subsequent water flooding was followed until the water cut was above 98%.

3 Principle of molecular designing

Based on the principle of compatibility with crude oil, the foaming agent was formulated that could achieve the ultra-low IFT and strong foamability simultaneously, so the betaine-type amphoteric surfactant is considered.

Firstly, to attain the ultra-low oil/water IFT, two key factors are necessary to be considered, firstly, the lipophilic groups of surfactant molecules should match the distribution of hydrocarbon composition in crude oil. Secondly, surfactant molecules are tightly arrayed and collected on the two-phase interface.

Therefore, analysis of crude oil from WX reservoir was carried out. The structural characterization of oil by FI-IR and ^{1}H NMR are shown in Supplementary Figures S1, S2, respectively. And the analysis of the hydrocarbon fraction of WX oil is investigated using GC-MS, as shown in Supplementary Figure S3.

According to the results of FI-IR spectroscopy of WX oil (Supplementary Figure S1), it is obvious that stretching vibrations and bending vibration of -CH_2- are exhibited at region ranges of 2,854~2,925 cm^{-1} and 1,557 cm^{-1}, respectively. The bending vibration of N-H bond and stretching vibration of C-N bond are found in 1,652 cm^{-1} and 1,040 cm^{-1}, respectively, it indicates that amidogen and acylamino linkage. In addition, the ^{1}H NMR spectra can be used to analyze the composition of the functional chemical groups. In Supplementary Figure S2, the characteristic signals at δ 0.97 ppm are attributed to the group of methyl (-CH3), while δ from 1.10 to 1.91 ppm are assigned to aliphatic methylene (-CH2-) and methine (-CH-). Besides, δ from 2.91 ppm to 3.50 ppm are indicative of aliphatic hydroxyl. δ from 3.24 to 3.57 ppm are assigned to hydroxyl group (-OH). The signals at δ 4.79 ppm are originated from the presence of D2O. Thus, the component of WX oil is mainly saturated hydrocarbon.

Moreover, in Supplementary Figure S3, it can be seen that WX oil was composed of straight and branched chain saturated hydrocarbons with carbon atoms ranging from C_7 to C_{36}, while it is mainly composed of straight chain hydrocarbons (C_{12}~C_{18}) with 61.32% normal paraffin contents.

As a result, the lipophilic group of surfactant molecule should be linear and branched aliphatic or alkyl chain that preferably having from 12 to 18 carbon atoms.

Secondly, to achieve a strong foamability, the hydrophilic group should include a sulfonic acid group (-SO_3^-) which have an excellent ability of hydration and anti-divalent ion (Hu et al., 2020). Doing so can efficiently improve the temperature-resistance and salinity-

TABLE 4 Summary of principle of molecule designing.

Key factors	Structure characteristics
attain the ultra-low IFT	①based on the principle of compatibility with crude oil, the lipophilic groups of surfactant molecules should match the distribution of hydrocarbon composition in crude oil
	② appropriately add the branched chain
excellent anti-hard water and temperature-resistant ability	structural formula: RO $(R'O)_xR''SO_3$-M^+ (Shupe and Maddox, 1981)
	-N^+-$(CH_3)_2$; avoid the group of -COOCH2- and -O-
	long- chain is mainly based on -C-C- or -C-N-bonds present
strong foamability	-SO_3^-
	-CONH-
	(R-$^+$N$(CH_3)_2$-$(CH_2)_n$ SO_3^-)

TABLE 5 Parameters of surface properties of C_n-HSB (n = 12~18) at 25°C.

Cn-HSB	CMC (mol/L)	γCMC (mN/m)	ΓCMC (μmol/m^2)	ACMC (nm^2)
C12	1.01×10^{-4}	35.36	5.16	0.322
C14	7.08×10^{-5}	31.94	4.88	0.340
C16	6.59×10^{-5}	29.76	4.72	0.352
C18	4.24×10^{-5}	25.36	4.22	0.393

resistance that is appropriate for application in high temperature and high salinity reservoirs.

In addition, the foamability and compatibility of betaine-type amphoteric surfactants can be further enhanced by introducing the amide group (-CONH-) and quaternary ammonium cationic group (-N^+-$(CH_3)_2$) (Fang, 1996). This is because the intermolecular hydrogen bond or dipole interaction between amide groups improves the molecular adsorption and arrangement on the surface, thus increasing the viscosity and elasticity of the adsorption layer and enhancing the stability of the adsorption film.

It has been reported in previous research that the best number of -CH_2- used to connect N and S is 3 in the chemical structure of sulphobetaine, in regard to the water solubility and LSDP (Lime Soap Dispersing Capability). Also, a modified sulphobetaine, exemplified by alkyl amide-hydroxysulfobetaine, has a good wettability, strong foamability and excellent anti-hard water performance.

As mentioned above, achieving the ultra-low IFT and strong foamability simultaneously allows the chemical flooding agent to be applicable to low permeability reservoirs, especially at high-temperature and high-sanity. The structural characteristic of molecular designing is given in Table 4. And the molecular structure of the amphoteric surfactant is shown in Supplementary Figure S4.

4 Results and analysis

4.1 The IFT and foam quality of different alkyl chain lengths of the Cn-HSB

The surface tension (SFT) of different alkyl chain lengths of the C_n-HSB (n = 12, 14, 16, 18) were measured by using the Du Noüy ring method. The plot of surface tension (γ) *versus* the logarithm of mass concentration ($\lg C$), is derived from γ-$\lg C$, which is shown in Supplementary Figure S5. It is observed that the γ is linearly correlated to $\lg C$ over a wide range, and the transition concentration is described as the CMC (critical micelle concentration). The CMC is an essential characteristic for surfactants, above which aggregates of surfactant molecules, so-called micelles, start to form. The value of CMC for C_n-HSB (n is from 12 to 18) solutions are 1.01×10^{-4} mol/L, 7.08×10^{-5} mol/L, 6.59×10^{-5} mol/L and 4.24×10^{-5} mol/L, respectively. Note that the value of CMC for C_n-HSB (n = 14~18) is one order of magnitude lower than that of C_{12}-HSB. Moreover, the C_{18}-HSB can be effectively decreased to 25.36 mN/m, which is lower compared to that of 35.36 mN/m, 31.94 mN/m and 29.76 mN/m for C_n-HSB (n is from 12 to 16). The longer the alkyl chain length of surfactant molecules, the lower the CMC value and the less effective the surface tension reduction. In general, repulsive electrostatic and van der Waals forces act as the two main interactive forces between surfactant molecules on the basis of DLVO theory. The increase in alkyl chain length enhances the interactive force between surfactant molecules, as well reduces the electrostatic repulsion between the hydrophilic headgroups of surfactant molecules, thereby leading to a denser monomolecular adsorption layer at the air/water interface and causing a higher surface concentration.

Also, to further investigate the electrostatic attraction, the maximum surface adsorption capacity (Γ_{CMC}) is calculated using Gibbs adsorption isothermal (Eq. 6) and the minimum area (A_{CMC}) occupied by per molecule at the water surface were obtained (Eq. 7). These results are shown in Supplementary Figure S6 and Table 5. It can be observed that with the increase of the chain length, the value of Γ_{CMC} decreases, which indicates that the adsorption efficiency of surfactant molecules at the gas/liquid interface decreases. The

TABLE 6 Elemental analysis of FI-IR data.

Trough	Wavenumber (cm^{-1})	Chemical group
1	3,424.88	-OH
2	2924.80	$-CH_3$
3	2854.20	$-CH_2-$
4	1633.57	-CONH-
5	1463.40	$-CH_2-$
6	1196.37	$-SO_3^-$
7	1043.32	-COO-
8	617.78	$-SO_3^-$

TABLE 7 Elemental analysis of ^{1}H NMR data.

Peak	Chemical shift (ppm)	n	Chemical group
a	0.87	3	$(-CH_3)$
b	1.15~1.31	24	$-(CH_2)m-$
c	1.56	2	$-CH_2-$
d	2.02~2.58	2	$-CH_2-CONH-$
l	2.04	1	-OH
f,h,i,j	3.26~3.81	14	-C-N-
k	3.77	1	-C-O-
m	4.71	2	$-CH_2-SO_3-$
e	7.73	1	-CONH-

surfactant molecules are arranged and collected more tightly on the two-phase interface, which leads to the increase of A_{CMC}.

$$\Gamma_{CMC} = -\frac{1}{2.303nRT} \times \frac{dy}{d\lg C} \quad (6)$$

$$A_{CMC} = -\frac{1}{N_A \cdot \Gamma_{CMC}} \quad (7)$$

Where C is the concentration of surfactant, mol/L;R is the gas equilibrium constant, R = 8.314J/(mol·K);T is absolute temperature, $T = t$+273.15°C, K;n is a constant, the value of which related to the number of solute species at the surface, herein, the value of n is taken as 2; N_A is Avogadro's constant, $N_A = 6.023\times10^{23}mol^{-1}$;

Subsequently, the EIFT, foam volume and half-life of different alkyl chain lengths of the C_n-HSB (n = 12~18) were conducted to evaluate the ability to reduce the IFT and foamability, as shown in Supplementary Figures S7, S8.

As is shown above (Supplementary Figures S7, S8), it can be seen that the shorter the chain, the higher the foaming qualities and the longer the chain, the lower the value of EIFT. The crude oil was composed of various lengths chain of saturated hydrocarbons with carbon atom. Thereby, to get the effective foaming agent that could achieve the ultra-low IFT and strong foamability simultaneously, inspect the combination of various lengths of the alkyl chain (C_n-HSB, n = 12, 14, 16, 18) with different molar ratios, as shown in Supplementary Figure S9. When C14:C16:C18 at the mixing ratios of 1.5:2:6.5, the oil/water IFT can achieve the lowest value, therefore, it was regarded as the best foaming agent for use in the subsequent experiment.

4.2 Characterization of the modified Cn-HSB

4.2.1 FI-IR

The FI-IR spectrum of modified C_n-HSB and the analytical results of FI-IR data are shown in Supplementary Figure S10 and Table 6. It can be seen that the obvious stretching vibrations of $-CH_2-$ and $-CH_3$ are all exhibited from 2,854–2,924 cm^{-1}, while the adsorption peaks at 3,424 cm^{-1} are assigned to the stretching of -OH. In fact, the movement of -OH from 3,650~3,600 cm^{-1} to a low wavenumber indicates the formation of hydrogen bonds (inter-OH group) in surfactant molecules. The stretching peaks of -CONH- and -COO- are found in 1,633 and 1,043 cm^{-1}, respectively. The peak at 1,196^{-1} and 620 cm^{-1} are also tentatively originated from the $-SO_3^-$ group. Thus, the FT-IR data confirms that the sulfonate group is successfully grafted onto the molecular chain structure of modified Cn-HSB surfactant.

4.2.2 ^{1}H NMR

The molecular structure of the modified C_n-HSB were further confirmed by ^{1}H NMR spectra as shown in Supplementary Figure S11 and the analysis of ^{1}H NMR data is in Table 7. The characteristic signals at δ 0.87 ppm is attributed to the group of methyl ($-CH_3$), while δ from 1.15 to 1.31 ppm are assigned to aliphatic methylene $(-CH_2-)_m$. In addition, δ from 3.26 to 3.81 ppm is indicative of (-C-N-). The signals from 2.02 to 2.58 ppm and at 7.73 ppm indicate the groups of (-CH2-CONH-) and -CONH-. δ 3.77 and 4.71 ppm are attributed to the group of (-C-O-) and (-CH2-SO3-), respectively. These peaks further confirm that modified Cn-HSB was successfully obtained.

4.3 Foam properties

The foam volume, half-life and *FCI* are used to qualitatively discuss the effect of the concentration of the foaming agent, TDS, temperature, and pressure on the stability of the foam, as shown in Supplementary Figure S12. It is observed that markedly increases in foam volume and foam half-life time both correlate with the increased concentration of the foaming agent, up to a concentration of 0.10*wt*%, at which point the increase becomes less pronounced. The foam volume and half-life are 448 mL and 2,567 s, respectively, at the concentration of 0.10*wt*%. Meanwhile, as can be seen from Supplementary Figures S12B, C, note that even though the values of the foam volume and half-life decrease with the TDS and temperature increase, the foam still is still maintained above 400 mL and 2,000 s, respectively (100°C, 154,929 mg/L). Therefore, the modified Cn-HSB has good thermal stability and excellent anti-hard water performance.

Moving on to the effects pressurization in the study, as shown in Supplementary Figures S12, S13, the higher the pressure, the better the foam qualities. In addition, the average radius of pore throat of WX reservoir is approximately 2 μm and the maximum wellhead injection pressure is 18.5 MPa. The bubble size is 1.879 μm under the high-pressure of 15 MPa, which means the injectivity of ultra-low IFT foam flooding is practical.

In conclusion, the modified foaming agent exhibits excellent foaming properties and foam stability.

Due to the long-term water flooding, the permeability of each flow unit is different, which leads to the great difference of TDS between reservoir layers. Therefore, it is necessary to investigate the influence of salinity on oil/water IFT to further explore the interfacial behavior and performance of modified Cn-HSB in reservoirs. The tests were conducted mainly under the conditions of TDS from 0 mg/L to 86,072 mg/L.

As can be seen from Supplementary Figure S14A the EIFT values first decreased at low TDS and then increased with the increase of TDS. This is because the ionic strength of aqueous solution can be increased through the "salt effect". At lower TDS, the ion hydration of the hydrophilic group of surfactant molecules decreased. As the TDS increases, the diffuse electric double layer is compressed and results in the greatly decrease of interface curvature. This subsequently causes more surfactant molecules to be collected onto the interface which has a positive impact on IFT reduction. However, at higher TDS, salts can reduce the solubility of surfactant that cause the precipitation and negative influence in IFT reduction. Nevertheless, it maintains the ultra-low value (the order of magnitude of 10^{-3} mN/m) that exhibit excellent salinity-resistance performance.

Supplementary Figure S14B shows the variant of DIFT with time. The DIFT initially dropped over time to the transient ultra-low IFT ($DIFT_{min}$), then increased slowly within the time period 15~60 min when equilibrium was finally established. The EIFT and $DIFT_{min}$ are 2.78 × 10^{-3} mN/m and 9.79 × 10^{-5} mN/m, respectively, at 86,072 mg/L concentration.

4.3.1 effect of temperature on IFT

Supplementary Figure S15 depicts the effect of temperature on the IFT of 0.10*wt*% modified C_n-HSB. It observed that the EIFT does not change substantially as temperatures rise, and the ultra-low EITF (the order of 10^{-3} mN/m) can be attained over a wide range of temperatures from 25°C to 100°C. The solubility of ionic surfactant in solution is enhanced with rising temperatures, parts of surfactant molecules were desorbed from the interface and dissolved into the aqueous solution, and the IFT increased slightly. As the temperature increases, the thermal motion of molecules is accelerated, as a result, the interaction forces between molecules are weakened. Meanwhile, the viscosity of the system is reduced, causing more molecules to be adsorbed and arranged on the interface, so the IFT again decreases slightly.

Foam, as a colloidal system (i.e., a dispersion of particles in a continuous medium) is establish by the particles of gas bubbles in a liquid medium. There are two main mechanisms contributing to the decay of foam: film drainage and gas diffusion. The rate of foam decay varies with the temperature, as is shown in Supplementary Figure S15A In the lower temperature range (25°C~45°C), the decay is mainly caused by gas diffusion. The increase of temperature accelerates the diffusion of gas and the evaporation of the liquid on the film. The film is thinned until it reaches a certain thickness as a result of film drainage when the Van der Waals force and repulsive force reach balance, as well due to the Gibbs–Marangoni effect, the foam is then metastable. At higher temperatures (˃45°C), the molecular movement is further intensified, accelerating the collision between bubbles, leading to the rupture of the liquid film and coalescence back into liquid medium, as such, the stability of the foam becomes worse. The intermolecular interaction also decreases with increased temperatures. As such, the adsorption quantity of molecules on the surface of the liquid film subsequently decreases while the A_{CMC} increases. In addition, as the Marangoni effect weakens, the film strength decreases.

The results discussed above indicated that the modified Cn-HSB can achieve the ultra-low IFT and strong foamability simultaneously.

4.4 Performance of oil displacement tests

In this part of study, a series of core flooding were carried out to investigate the injectivity and displacement efficiency of ultra-low foam flooding, as shown in Table 8.

TABLE 8 Properties of low permeability cores, the oil displacement efficiency and residual oil saturation.

Core	*L* (cm)	*D* (cm)	ϕ (%)	*k* (×10^{-3}μm^2)	Oil saturation (%)	Water-flooding recovery (%)	Oil displacement efficiency (%)	Residual oil saturation (%)
F1	5.13	2.45	0.79	0.08	45.03	34.33	1.79	29.10
F2	5.52	2.45	1.29	0.14	45.97	35.21	2.31	29.18
F3	5.25	2.45	1.89	0.25	46.92	37.85	3.94	28.32
F4	6.03	2.45	2.76	0.58	48.78	40.46	7.68	27.92
F5	6.17	2.45	6.55	0.91	47.86	44.89	9.63	24.49
F6	6.25	2.45	12.68	1.50	49.91	45.71	12.54	23.26
F7	6.01	2.45	14.36	2.27	50.71	46.57	16.16	22.21
F8	5.35	2.45	14.38	5.39	54.17	48.07	16.51	21.34
F9	5.10	2.45	16.44	8.04	57.21	47.95	16.93	20.53
F10	5.25	2.45	17.57	14.98	59.75	48.89	17.03	20.67
F11	5.09	2.45	19.35	33.38	59.87	49.33	17.10	20.20
F12	5.44	2.45	20.61	51.51	62.16	50.47	17.15	20.13

Where *L* is length; *D* is diameter; ϕ is porosity; *k* is the permeability.

As mentioned above, when $\Delta P \geq P_c$, that is $\frac{dP}{dx} \cdot L > \frac{2\sigma \cos\theta}{r}$, the capillary trapped residual oil can be mobilized. As such, there exists a critical permeability which greatly improves the oil displacement efficiency.

In reference to Supplementary Figure S16, there is an obvious S-curve for the permeability and oil displacement efficiency. Conversely, the curve of the permeability and residual oil saturation displays an inverse S-curve. Critical permeability is reached at the point when the oil displacement efficiency plateaus despite a continued increase in permeability. The critical permeability of ultra-low foam flooding is $2.27 \times 10^{-3}\mu m^2$, at which point, the oil displacement efficiency is 16.16%.

The injectivity of ultra-low foam flooding is shown in Supplementary Figure S17. The relationship between permeability and threshold pressure gradient of ultra-low foam flooding is expressed by $y = 0.202x^{-0.595}$ that the correlation coefficient is 0.977. As can be seen in Supplementary Figure S17, when $k \leq 1.50 \times 10^{-3}\mu m^2$, the threshold pressure gradient rapidly increased with the decrease of permeability, which from 0.72 MPa/m at $k = 0.143 \times 10^{-3}\mu m^2$ to 0.115 MPa/m at $k = 1.50 \times 10^{-3}\mu m^2$. Under conditions $1.50 \times 10^{-3}\mu m^2 < k < 14.98 \times 10^{-3}\mu m^2$, the threshold pressure gradient slightly decreased with the increase of permeability, from 0.115 to 0.041 MPa/m. When conditions reached $k \geq 14.98 \times 10^{-3}\mu m^2$, the threshold pressure gradient levels off.

Moreover, when $k = 1.0 \times 10^{-3}\mu m^2$ equals, the threshold pressure gradient can be calculated by $y = 0.202x^{-0.595}$, it is 20.2 MPa/100 m. In general, the distance between wells is usually 70~200 m, which means the ultra-low foam flooding has ideal injectivity in low permeability reservoirs.

Moreover, the artificial core samples were used to research the effect of wettability on oil displacement efficiency, as shown in Supplementary Figure S18. The tendency of the curves has the similar variation with Supplementary Figure S16.

It is clearly observed in Supplementary Figure S19, that the critical permeability increases with the increase of contact angle, the semilogarithmic coordinates express a linear distribution. When the contact angle is 18°, 44°, 78° and 142°, respectively, the corresponding critical permeability is $33.38 \times 10^{-3}\mu m^2$, $6.13 \times 10^{-3}\mu m^2$, $1.97 \times 10^{-3}\mu m^2$ and $0.15 \times 10^{-3}\mu m^2$, respectively. Therefore, the more the reservoir rock trends to water wettability, the lower the critical permeability must be for mobilizing the capillary trapped residual oil.

5 Conclusion

The following conclusions were drawn based on the laboratory results:

(1) A modified Cn-HSB as a foaming agent based on the principle of compatibility with crude oil was formulated that could achieve the ultra-low IFT and strong foamability simultaneously, which could reduce the oil/water dynastic IFT to an ultra-low value of the order of 10^{-5} mN/m (0.10*wt*%), as well as the foam volume and half-life are 448 mL and 2,567 s, respectively, under the conditions of WX reservoirs (84°C, 86,072 mg/L).

(2) The ultra-low foam flooding was shown to be successful to mobilize the trapped oil in low permeability porous media ($k = 1.50 \times 10^{-3}\mu m^2$) when the threshold pressure gradient is 0.115 MPa/m, which improves oil displacement efficiency approximately15%OOIP.

(3) The more the reservoir rock trends to water wettability, the lower the critical permeability must be for mobilizing the capillary trapped residual oil. When the contact angle is 18°, 44°, 78° and 142°, respectively, the corresponding critical permeability are 33.38×10^{-3}, 6.13×10^{-3}, 1.97×10^{-3} and $0.15 \times 10^{-3}\mu m^2$, respectively.

Data availability statement

The original contributions presented in the study are included in the article/Supplementary Material, further inquiries can be directed to the corresponding authors.

Author contributions

LL: Writing–review and editing, Writing–original draft. SZ: Writing–review and editing, Writing–original draft. LL: Writing–review and editing, Writing–original draft.

Funding

The author(s) declare that no financial support was received for the research, authorship, and/or publication of this article.

Conflict of interest

Authors LL, SZ, and LL were employed by SINOPEC Southwest Oil and Gas Company.

Publisher's note

Supplementary material

The Supplementary Material for this article can be found online at: https://www.frontiersin.org/articles/10.3389/fenrg.2024.1370970/full#supplementary-material

References

Cambridge, V. J., Wolcott, J. M., and Constant, W. D. (1989). An investigation of the factors influencing trans ent interfacial tension behavior in crude oil/alkaline water systems. *Chem. Eng. Commun.* 84 (01), 97–111. doi:10.1080/00986448908940337

Hu, R., Tang, S., Mpelwa, M., Jin, L., Deng, H., Feng, S., et al. (2020). A new low interfacial tension viscoelastic surfactant for EOR applications in low permeability reservoirs. *J. Appl. Sci. Eng.* 23 (04), 701–711. doi:10.6180/jase.202012_23(4).0015

Li, Z., Wu, H., Hu, Y., Chen, X., Yuan, Y., Luo, Y., et al. (2020). Ultra-low interfacial tension biobased and catanionic surfactants for low permeability reservoirs. *J. Mol. Liq.* 309, 113099. doi:10.1016/j.molliq.2020.113099

Rubin, E., and Radke, C. J. (1980). Dynamic interfacial tension minima in finite systems. *Chem. Eng. Sci.* 35 (05), 1129–1138. doi:10.1016/0009-2509(80)85102-5

Sharma, M. M., Jang, L. K., and Yen, T. F. (1989). Transient interfacial tension behavior of crude-oil/caustic interfaces. *SPE Reserv. Eng.* 4 (02), 228–236. doi:10.2118/12669-pa

Shupe, R. D., and Maddox, J., Jr. (1981). *Emulsion oil recovery process usable in high temperature, high salinity formations*. US Patent 4269271.

Taylor, K. C., and Schramm, L. L. (1990). Measurement of short-term low dynamic interfacial tensions: application to surfactant enhanced alkaline flooding in enhanced oil recovery. *Colloids Surfaces* 47, 245–253. doi:10.1016/0166-6622(90)80076-g

Trujillo, E. M. (1983). The static and dynamic interfacial tensions between crude oils and caustic solutions. *SPE J.* 23 (04), 645–656. doi:10.2118/10917-pa

Wang, D. M., and Cheng, J. C. (2001). "Successful field test of the first ultra-low interfacial tension foam flood," in SPE Asia Pacific Improved Oil Recovery Conference, Kuala Lumpur, Malaysia, October, 2001.

Yu, W., Lashgari, H. R., Kan, W., and Sepehrnoori, K. (2015). CO_2 injection for enhanced oil recovery in Bakken tight oil reservoirs. *Fuel* 159, 354–363. doi:10.1016/j.fuel.2015.06.092